Wall-vortex composite solitons in two-component Bose-Einstein condensates

Kenichi Kasamatsu,[1] Hiromitsu Takeuchi,[2] Makoto Tsubota,[2,3] and Muneto Nitta[4]

[1]*Department of Physics, Kinki University, Higashi-Osaka 577-8502, Japan*

[2]*Department of Physics, Osaka City University, Sumiyoshi-ku, Osaka 558-8585, Japan*

[3]*The OCU Advanced Research Institute for Natural Science and Technology (OCARINA), Osaka City University, Sumiyoshi-ku, Osaka 558-8585, Japan*

[4]*Department of Physics, and Research and Education Center for Natural Sciences, Keio University, Hiyoshi 4-1-1, Yokohama, Kanagawa 223-8521, Japan*

(Received 28 March 2013; published 15 July 2013)

We study composite solitons, consisting of domain walls and vortex lines attaching to the walls in two-component Bose-Einstein condensates. When the total density of the two components is homogeneous, the system can be mapped to the O(3) nonlinear σ model for the pseudospin representing the two-component order parameter, and the analytical solutions of the composite solitons can be obtained. Based on the analytical solutions, we discuss the detailed structure of the composite solitons in two-component condensates by employing the generalized nonlinear σ model, where all degrees of freedom of the original Gross-Pitaevskii theory are active. The domain wall pulled by a vortex is logarithmically bent as a membrane pulled by a pin. It bends more flexibly than the domain wall in the σ model, because the density inhomogeneity results in a reduction of the domain wall tension from that in the σ model limit. We find, however, that the curvature of the wall bending pulled by a vortex is still greater than that expected from the reduced tension due to only the density inhomogeneity. Finally, we study the composite soliton structure for actual experimental situations with trapped immiscible condensates under rotation, through numerical simulations of the coupled Gross-Pitaevskii equations.

DOI: 10.1103/PhysRevA.88.013620 PACS number(s): 03.75.Lm, 03.75.Mn, 05.30.Jp, 67.85.Fg

I. INTRODUCTION

Topological defects or topological solitons are solutions of systems obeying partial differential equations, and represent localized structures with their stability being attributable to nontrivial topology [1]. Vortices in superfluids and superconductors are an example of line topological defects [2], and it is believed that the analogous defects exist in the early universe as cosmic strings [3]. A domain wall is a planar topological defect separating two different vacua or phases. When a symmetry group G of a system is spontaneously broken into a subgroup H, the topologically allowed defect type is determined by the homotopy properties of the order parameter space (vacuum manifold) G/H. In a $(d+1)$-dimensional space-time, p-dimensional defects ($p < d$) exist if the homotopy group $\pi_{d-p-1}(G/H)$ is nontrivial. Thus, for $d = 3$, planar defects (domain walls) can be expected if $\pi_0(G/H) \neq 0$, linear defects (vortices or strings) can be expected if $\pi_1(G/H) \neq 0$, and point defects (monopoles) can be expected if $\pi_2(G/H) \neq 0$. These defects can be classified as "singular" or "continuous" in the sense of whether (a part of) G is recovered at the core of the defects. The order parameter is not defined at the core of a singular defect, but it is defined everywhere for a continuous texture (defects).

Bose-Einstein condensates (BECs) of ultracold atomic gases provide an ideal system for examining topological solitons in a quantum condensed system [4]. A major advantage of this system is that the properties of BECs can be quantitatively described by using mean-field theory, namely, the Gross-Pitaevskii (GP) model. From an experimental point of view, cold-atom BECs are a versatile system to study topological defects, because most of the system parameters are tunable and optical techniques allow one to engineer the condensate wave function as well as to visualize the condensates directly. In the context of a single-component BEC characterized by a scalar order parameter with broken U(1) symmetry, there are many papers discussing the properties of solitons and vortices; see Refs. [5,6] for reviews. In addition, realization of multicomponent (spinor) BECs with multiple order parameters provides a ground to study more complex topological solitons [7], as studied in superfluid ^{3}He [8]. For example, dark-bright solitons can be excited in two-component BECs [9,10], where a dark soliton (density dip) of one component can trap a bright soliton (density hump) of the other component [11]. Exotic vortices composed of several order parameter components have been observed experimentally [12–16]. Because the order parameter space of multicomponent BECs can possess higher symmetry than U(1) of the scalar BEC, their homotopy groups π_n with different n can become simultaneously nontrivial and thus different types of topological solitons can coexist. There has been discussion of the structure, stability, and creation and detection schemes for various types topological solitons in multicomponent BECs, including monopoles [17–21], three-dimensional (3D) skyrmions [22–27], cosmic vortons [28,29], and knots [30,31].

In this paper, we discuss a 3D composite soliton consisting of domain walls and vortices in immiscible two-component BECs, as sketched in Fig. 1. Two-component BECs have been realized by using a mixture of atoms with two hyperfine states of ^{87}Rb [32–35] or a mixture of two different species of atoms such as ^{87}Rb-^{41}K [36,37], ^{85}Rb-^{87}Rb [38], or ^{87}Rb-^{133}Cs [39]. Experiments [35,38] have demonstrated that miscibility and immiscibility of two-component BECs can be controlled by tuning the atom-atom interaction via Feshbach resonances. The domain wall is referred to as a boundary of the phase-separated two-component BECs and is well defined as a plane on which both components have the same amplitudes [40–43]. The vortices can be arranged by applying rotation of

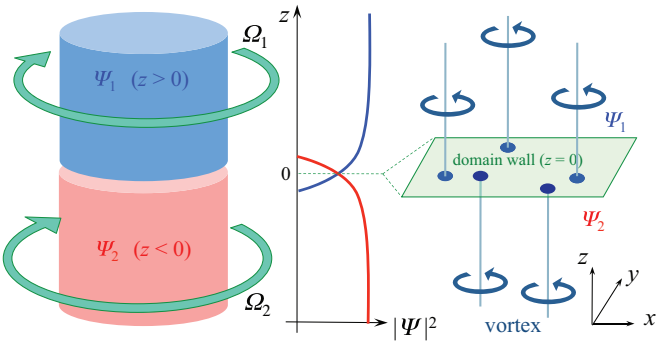

FIG. 1. (Color online) Schematic illustration of the wall-vortex soliton configuration in two-component BECs. The two-component BECs Ψ_1 at $z>0$ and Ψ_2 at $z<0$ are separated by the domain wall at the $z=0$ plane. Since penetration of the condensate densities takes place around the boundary, the domain wall is well defined as a plane on which both components have the same amplitude, as shown in the middle panel. We assume that vortex lines are straight and perpendicular to the wall. Rotation is applied to the two components with a different rotation frequency $\mathbf{\Omega}_i = \Omega_i \hat{\mathbf{z}}$.

the confining potential around the z axis to the phase-separated BECs [6]. We assume that the two components undergo phase separation in the $z>0$ and $z<0$ regions, forming a domain wall lying at the $z=0$ plane with edges of the vortex lines along the z axis attaching to the domain wall.

In our previous paper [44], we pointed out that the wall-vortex composite soliton in two-component BECs can be identified as a nonrelativistic analog of the "Direchlet (D)-brane soliton" found in some field theoretical models [45–49]. This statement is based on the fact that the GP equations for two-component BECs can be mapped to the O(3) nonlinear σ model (NLσM) by introducing a pseudospin representation of the order parameter [50–52]. NLσM admits a solitonic object that can have properties similar to those of the D-brane in string theory [45]. The purpose of this paper is to discuss in more detail the structure of this composite soliton in two-component BECs. The generalized NLσM for two-component BECs includes additional degrees of freedom compared with the original O(3) NLσM, which modifies some properties of the composite soliton known in the previous literature. (i) Vortices consisting of a composite soliton have a singular core, whereas they are nonsingular in NLσM. (ii) The density inhomogeneity of the BECs results in reduction of the domain wall tension from that in NLσM. (iii) The domain wall attached by a vortex is logarithmically bent, as a membrane pulled by a pin, and it bends more flexibly than the domain wall in NLσM. However, the reduced tension caused by (ii) is insufficient to account for the observed curvature of the domain wall bending in the presence of a vortex. We also study the composite soliton structure of rotating immiscible BECs in a trapping potential through 3D numerical simulations of the coupled GP equations. To reduce the gradient energy of the density, the domain wall tends to be parallel to the rotation axis and forms a vortex sheet [53]. At high rotation frequency, a lattice of two-dimensional (2D) skyrmions can form upon the domain wall, which undergoes triangular or rectangular ordering caused by the effective intercomponent repulsion realized in the restricted system on the domain wall.

This paper is organized as follows. In Sec. II, we formulate the problem for two-component BECs and introduce the pseudospin representation to reduce the GP model to NLσM. In Sec. III, we examine the structure of wall-vortex composite solitons based on the analysis of NLσM, where analytic solutions of these solitons can be obtained. In Sec. IV, we discuss how the composite solitons in two-component BECs are modified from the analytic solutions in NLσM and present the results of 3D numerical simulations for the trapped immiscible two-component BECs under rotation. We conclude this paper in Sec. V.

II. THEORETICAL FORMULATION OF TWO-COMPONENT BECS

We study the detailed properties of composite solitons in two-component BECs, whose basic configuration is illustrated schematically in Fig. 1. Two-component BECs are represented by the order parameters $(\Psi_1,\Psi_2)^T = (\sqrt{\rho_1}e^{i\theta_1},\sqrt{\rho_2}e^{i\theta_2})^T$, which are the condensate wave functions with density ρ_j and phase θ_j $(j=1,2)$. They are confined in some trapping potentials and undergo phase separation, which results in the domain walls. The quantized vortices can exist in each component, being created by rotating the system or imprinting the circulating phase by atom-laser coupling [6]. We first show that the theoretical formulation of this system can be mapped to NLσM. This mapping was first discussed in the two-component Ginzburg-Landau theory for charged two-component Bose systems [54], which was applied to two-component BECs by some of the authors [50,51].

The solitonic structure in two-component BECs is given by the analysis of the two-component GP model. The energy functional is given by

$$E[\Psi_1,\Psi_2] = \int d\mathbf{r} \left\{ \sum_{j=1,2} \left[\frac{\hbar^2}{2m_j} \left| \left(\nabla - i\frac{2m_j}{\hbar}\tilde{\mathbf{A}} \right) \Psi_j \right|^2 + (V_j - \mu_j)|\Psi_j|^2 + \frac{g_{jj}}{2}|\Psi_j|^4 \right] + g_{12}|\Psi_1|^2|\Psi_2|^2 \right\}. \quad (1)$$

Here m_j and μ_j are the mass and the chemical potential, respectively, of the jth component. The trapping potential is expressed with an axisymmetric harmonic oscillator as

$$V_j = \tfrac{1}{2}m_j\omega_j^2(r^2+\lambda^2 z^2), \quad (2)$$

with an aspect ratio λ, where $\lambda<1$ (>1) represents a cigar-shaped (pancake-shaped) potential. The coefficients g_{11}, g_{22}, and g_{12} represent the atom-atom interactions. They are expressed in terms of the s-wave scattering lengths a_{11} and a_{22} between atoms in the same component and a_{12} between atoms in different components as

$$g_{jk} = \frac{2\pi\hbar^2 a_{jk}}{m_{jk}}, \quad (3)$$

with $m_{jk}^{-1} = m_j^{-1} + m_k^{-1}$. The vector potential $\tilde{\mathbf{A}}$ is generated by (i) the rotation of the system $\tilde{\mathbf{A}} = (\mathbf{\Omega}\times\mathbf{r})/2$ [6] or (ii) a

synthesis of the artificial magnetic field by the laser-induced Raman coupling between the internal hyperfine states of the atoms [55].

The two-component GP model can be transformed into a form similar to that of NLσM by introducing the pseudospin representation of the order parameter. Here we confine ourselves to the simple situation with equal masses $m_1 = m_2 = m$ and equal trapping frequencies $\omega_1 = \omega_2 = \omega$; its derivation in the case of the general parameters of the system, e.g., the mass imbalance and the difference of the trapping frequencies, was considered by Mason and Aftalion [52]. The condensate wave functions are denoted as

$$\begin{pmatrix} \Psi_1 \\ \Psi_2 \end{pmatrix} = \sqrt{\rho} e^{i\Theta/2} \begin{pmatrix} \zeta_1 \\ \zeta_2 \end{pmatrix}. \tag{4}$$

Here $\zeta = [\zeta_1, \zeta_2]^T$ is the spin-$\frac{1}{2}$ spinor with $|\zeta_1|^2 + |\zeta_2|^2 = 1$. The four degrees of freedom of the original wave functions $\Psi_j = \sqrt{\rho_j} e^{i\theta_j}$ (of amplitudes ρ_j and phases θ_j) are expressed in terms of the total density $\rho = \rho_1 + \rho_2$, the total phase $\Theta = \theta_1 + \theta_2$, and the polar angle θ and azimuthal angle ϕ of the local pseudospin $\mathbf{s} = (s_x, s_y, s_z)$ defined as

$$\mathbf{s} = \zeta^\dagger \boldsymbol{\sigma} \zeta = \begin{bmatrix} \zeta_1^* \zeta_2 + \zeta_2^* \zeta_1 \\ -i(\zeta_1^* \zeta_2 - \zeta_2^* \zeta_1) \\ |\zeta_1|^2 - |\zeta_2|^2 \end{bmatrix} = \begin{bmatrix} \sin\theta \cos\phi \\ \sin\theta \sin\phi \\ \cos\theta \end{bmatrix}, \tag{5}$$

where $\boldsymbol{\sigma}$ is the Pauli matrix, $\cos\theta = (\rho_1 - \rho_2)/\rho, \phi = \theta_2 - \theta_1$, and $|\mathbf{s}|^2 = 1$. By using these variables, the total energy, Eq. (1), can be rewritten in the form of the generalized NLσM [51]:

$$E = \int d\mathbf{r} \left\{ \frac{\hbar^2}{2m} \left[(\nabla\sqrt{\rho})^2 + \frac{\rho}{4} \sum_\alpha (\nabla s_\alpha)^2 \right] + V\rho + \frac{m\rho}{2} v_{\text{eff}}^2 + U(\rho, s_z) \right\}, \tag{6}$$

where we have introduced the effective velocity field $\mathbf{v}_{\text{eff}} = \mathbf{v}_g + \mathbf{v}_s - 2\tilde{\mathbf{A}}$, which arises from the gradient of the total phase,

$$\mathbf{v}_g = \frac{\hbar}{2m} \nabla\Theta, \tag{7}$$

and the flux flow of the spinor,

$$\mathbf{v}_s = \frac{\hbar}{2mi} \sum_{j=1,2} (\zeta_j^* \nabla \zeta_j - \zeta_j \nabla \zeta_j^*) = \frac{\hbar}{2m} \frac{s_z}{s_x^2 + s_y^2} (s_y \nabla s_x - s_x \nabla s_y) = -\frac{\hbar}{2m} \cos\theta \nabla\phi. \tag{8}$$

Here we have also used the relation

$$\frac{\hbar^2}{2m} (|\nabla\zeta_1|^2 + |\nabla\zeta_2|^2) - \frac{v_s^2}{4} = \frac{\hbar^2}{8m} \sum_\alpha (\nabla s_\alpha)^2. \tag{9}$$

The second term on the right-hand side of Eq. (6) corresponds to the classical NLσM for a Heisenberg ferromagnet. The generalized NLσM has several unique features. (i) There is a gradient term of the total density. (ii) The spin stiffness, a prefactor of the $(\nabla s_\alpha)^2$ term, depends on the total density ρ and is generally spatially inhomogeneous. (iii) There is an additional kinetic-energy term, $m\rho v_{\text{eff}}^2/2$, associated with the presence of the superfluid velocity $\mathbf{v}_{\text{eff}} \neq 0$ and the external vector potential $\tilde{\mathbf{A}} \neq 0$.

The potential U is a function of the total density ρ and the z component s_z of the pseudospin only, being explicitly written as

$$U(\rho, s_z) = c_0 + c_1 s_z + c_2 s_z^2, \tag{10}$$

with

$$c_0 = \frac{\rho}{8} [\rho(g_{11} + g_{22} + 2g_{12}) - 4(\mu_1 + \mu_2)], \tag{11}$$

$$c_1 = \frac{\rho}{4} [\rho(g_{11} - g_{22}) - 2(\mu_1 - \mu_2)], \tag{12}$$

$$c_2 = \frac{\rho^2}{8} (g_{11} + g_{22} - 2g_{12}). \tag{13}$$

If $g_{11} \neq g_{22} \neq g_{12}$ or $\mu_1 \neq \mu_2$, the anisotropic terms with coefficients c_1 and c_2 break the global SU(2) invariance of the system. The coefficient c_1 can be interpreted as a longitudinal magnetic field that tends to align the pseudospin along the z axis. The term with coefficient c_2 determines the spin-spin interaction associated with s_z; it is antiferromagnetic for $c_2 > 0$ and ferromagnetic for $c_2 < 0$ [51]. The stationary point of this potential gives the equilibrium values

$$\rho = \frac{(g_{22} - g_{12})\mu_1 + (g_{11} - g_{12})\mu_2}{g_{11}g_{22} - g_{12}^2}, \tag{14}$$

$$s_z = \frac{(g_{22} + g_{12})\mu_1 - (g_{11} + g_{12})\mu_2}{(g_{22} - g_{12})\mu_1 + (g_{11} - g_{12})\mu_2}. \tag{15}$$

The determinant of the Hessian at that point is given by

$$\frac{\partial^2 U}{\partial\rho^2} \frac{\partial^2 U}{\partial s_z^2} - \left(\frac{\partial^2 U}{\partial s_z \partial\rho} \right)^2 = \frac{[(g_{22} - g_{12})\mu_1 + (g_{11} - g_{12})\mu_2]^2}{4(g_{11}g_{22} - g_{12}^2)}. \tag{16}$$

The stationary point is a minimum or a maximum only when $g_{11}g_{22} - g_{12}^2 > 0$. Otherwise, the minimum of the potential disappears within the range $-1 < s_z < 1$ and the degenerate energy minima are given by $s_z = 1$ or $s_z = -1$. This situation corresponds to ferro-magnetization, namely, the phase separation of the two-component BECs, which is discussed in the following text.

III. TOPOLOGICAL SOLITONS IN THE NONLINEAR σ MODEL

To understand the properties of a wall-vortex soliton in a field theoretical model, we consider static solutions of the topological solitons in the O(3) NLσM [45]. NLσM is a scalar field theory whose (multicomponent) scalar field defines a map from a "space-time" to a Riemann (target) manifold. The energy functional is given as

$$E[\mathbf{s}] = \frac{1}{4} \int d\mathbf{r} \left[\sum_{\alpha=1}^{3} (\nabla s_\alpha)^2 + U(\mathbf{s}) \right], \tag{17}$$

which is also known as the Landau-Lifshitz model governing the high-spin and long-wavelength limit of ferromagnetic materials. Here the amplitude of the vector is $|\mathbf{s}(\mathbf{r})| = 1$ at all instances. The ground state is twofold degenerate, for example, $s_z = +1$ and -1, where the potential can be described as

$$U(\mathbf{s}) = m_\sigma^2 (1 - s_z^2), \tag{18}$$

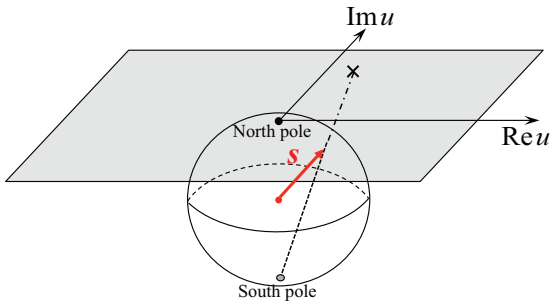

FIG. 2. (Color online) Stereographic projection from the sphere to the tangent plane at the north pole.

with mass parameter m_σ. This massive NLσM given by Eq. (17) is essentially equivalent to the truncated version of the massive hyper-Kähler σ model employed in Ref. [45], where the analytical solitonic solutions were derived from this truncated model.

Under several conditions, our model [Eq. (6)] can be reduced to the same form as Eq. (17) [44]. For a simple situation, we consider a homogeneous system without a trapping potential ($V = 0$) and set the parameters as $g_{11} = g_{22} \equiv g$ and $\mu_1 = \mu_2 \equiv \mu$. The anisotropy coefficient c_1 in Eq. (10) then vanishes and the total energy can be written as

$$E = \int d\mathbf{r}\left\{\frac{\hbar^2}{2m}\left[(\nabla\sqrt{\rho})^2 + \frac{\rho}{4}\sum_\alpha(\nabla s_\alpha)^2\right] + \frac{m\rho}{2}v_{\rm eff}^2 + \frac{g}{2}\left(\rho - \frac{\mu}{g}\right)^2 - \frac{g - g_{12}}{4}\rho^2\left(1 - s_z^2\right)\right\}, \tag{19}$$

where the constant term has been omitted. The coefficient of the last term in Eq. (19) is positive because we consider the case of $g_{12} > g$, giving the mass for the s_z field. In the limit $g \to \infty$, which corresponds to the Thomas-Fermi limit [4], we can approximate that the total density is fixed at $\rho = \mu/g \equiv \rho_0$ and that the $(\nabla\sqrt{\rho})^2$ term vanishes. The kinetic energy associated with the superflow $\mathbf{v}_{\rm eff}$ is assumed to be negligible for simplicity [56]. By using the healing length $\xi = \hbar/\sqrt{2mg\rho_0}$ as the length scale, the total energy reduces to

$$\tilde{E} = \frac{E}{g\rho_0^2\xi^3} \simeq \frac{1}{4}\int d\mathbf{r}\left[\sum_\alpha(\nabla s_\alpha)^2 + m_\sigma^2\left(1 - s_z^2\right)\right], \tag{20}$$

with mass

$$m_\sigma^2 \equiv \left|1 - \frac{g_{12}}{g}\right|. \tag{21}$$

Therefore, the following discussion based on Eq. (17) can be applied approximately to our system. Actually, as explained later, the additional degrees of freedom in a two-component BEC system yield only a quantitative modification of the soliton structure.

To this end, we introduce the stereographic coordinate

$$u = \frac{s_x + is_y}{1 + s_z}, \tag{22}$$

where $u = 0$ (∞) corresponds to the north (south) pole of the spin sphere, as shown in Fig. 2. Then each component of the pseudospin is written as

$$(s_x, s_y, s_z) = \left(\frac{u + u^*}{1 + |u|^2}, -i\frac{u - u^*}{1 + |u|^2}, \frac{1 - |u|^2}{1 + |u|^2}\right) \tag{23}$$

and Eq. (17) becomes

$$E = \int d^3x \frac{\sum_\alpha |\partial_\alpha u|^2 + m_\sigma^2|u|^2}{(1 + |u|^2)^2}. \tag{24}$$

The solutions of the topological solitons can be obtained by taking the Bogomol'nyi-Prasad-Sommerfield (BPS) bound for the total energy [57,58]. Often, by enforcing the case that the bound is satisfied ("saturated"), one can obtain a simpler set of partial differential equations to solve the Bogomol'nyi equations by completing the square. Solutions saturating the bound are called BPS states, and their energy is proportional to a topological charge that characterizes the solitons. Here we summarize the properties of the BPS saturated solutions of the topological solitons.

A. Vortex configuration

In the case of $m_\sigma = 0$ in Eq. (17), the Hamiltonian of the system has O(3) symmetry. Because the symmetry of the ground state is broken to O(2), the order parameter space is $G/H = {\rm O}(3)/{\rm O}(2) \simeq S^2$. Then the second homotopy group is nontrivial as $\pi_2(S^2) = \mathbf{Z}$. This suggests the presence of pointlike defects such as monopoles and 2D nonsingular defects such as "2D skyrmions" (coreless vortices) [15,16], because the former configuration can be mapped to the latter through stereographic projection.

First, we derive the analytic solutions of the coreless vortices by taking the BPS bound. We restrict ourselves to consider static solutions that are translationally invariant along the z axis. The total energy can be written as

$$E = \int d^2x \frac{\partial_x u\partial_x u^* + \partial_y u\partial_y u^*}{(1 + |u|^2)^2} = 2\int d^2x \frac{|\partial_w u|^2 + |\partial_{\bar{w}} u|^2}{(1 + |u|^2)^2}, \tag{25}$$

where we have introduced $w = x + iy$, $\partial_w = (\partial_x - i\partial_y)/2$, and $\partial_{\bar{w}} = (\partial_x + i\partial_y)/2$. The topological charge $T_{\rm v} \in \pi_2(S^2) = \mathbf{Z}$ of the coreless vortices is given by the number of times that $\mathbf{s}$ (or u) winds around S^2. By considering the normalized area element of S^2, i.e., $[(\nabla\theta) \times (\sin\theta\nabla\phi)] \cdot d\mathbf{S}/4\pi$, such a winding number can be expressed as

$$T_{\rm v} = \frac{1}{4\pi}\int [(\nabla\theta) \times (\sin\theta\nabla\phi)] \cdot d\mathbf{S} = \frac{1}{8\pi}\int [\epsilon_{\alpha\beta\gamma}s_\alpha(\nabla s_\beta) \times (\nabla s_\gamma)] \cdot d\mathbf{S}, \tag{26}$$

with the infinitesimal plane $d\mathbf{S}$ and the Levi-Civita symbol $\epsilon_{\alpha\beta\gamma}$. By using the relation $u = \tan(\theta/2)e^{i\phi}$ or Eq. (23), $T_{\rm v}$ can be rewritten in terms of u as

$$T_{\rm v} = \frac{1}{\pi}\int d^2x \frac{|\partial_w u|^2 - |\partial_{\bar{w}} u|^2}{(1 + |u|^2)^2}. \tag{27}$$

By substituting with Eq. (27) in Eq. (25), we find that the total energy can be written as the sum of the topological charge and

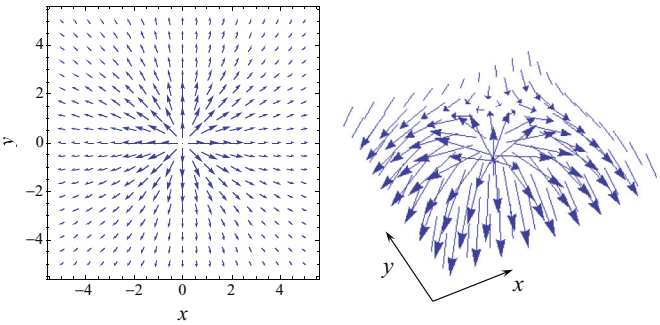

FIG. 3. (Color online) Spin profile of a coreless vortex. The spin component is given by $(s_x,s_y,s_z) = (2x/(1+r^2),2y/(1+r^2),(1-r^2)/(1+r^2))$.

a positive correction:

$$E = 2\pi T_{\rm v} + 4\int d^2x \frac{|\partial_{\bar{w}} u|^2}{(1+|u|^2)^2}. \tag{28}$$

Thus, the energy is bounded by the topological charge $E \geqslant 2\pi T_{\rm v}$ and the equality holds only if

$$\partial_{\bar{w}} u = 0. \tag{29}$$

This equation is called a Bogomol'nyi equation. It is a first-order equation whose solution gives a field configuration with a minimal energy within a fixed topological sector $T_{\rm v}$. Equation (29) also shows that u is a holomorphic function of w only. Note that u is allowed to have a pole at any point $w = w_i$ because its image on the target S^2 is simply the south pole. The requirement that the total energy is finite, together with the boundary condition that u has a definite limit as $|w| \to \infty$, forces u to be a rational map:

$$u_{\rm v}(w) = \frac{f(w)}{g(w)} = \frac{\prod_{i=1}^{N_n}(w-w_i^n)}{\prod_{i=1}^{N_s}(w-w_i^s)}, \tag{30}$$

where f and g are polynomials in w with no common factors. This solution gives the vortex configuration, in which $f(w)$ and $g(w)$ represent N_n vortices (north poles) and N_s antivortices (south poles), respectively. The positions of the vortices are denoted by w_i^n and w_i^s. We note that the total energy does not depend on the form of the solution, but only on the topological charges. In NLσM, the energy is independent of the vortex positions $w_i^{n,s}$; in other words, there is no static interaction between vortices.

Figure 3 represents the profile of the spin field for the simple vortex solution $u_{\rm v}(w) = w$. The spin orients upward at the center ($s_z \to 1$ as $|w| \to 0$) and it continuously rotates in the up and down direction as it moves outward radially ($s_z \to -1$ as $|w| \to \infty$). The spin configuration of this continuous (coreless) vortex is known as a lump in field theory [59], an Anderson-Toulouse vortex in superfluid ^{3}He [60], or a 2D skyrmion in spinor BECs [15,16].

B. Domain wall

Next, let us consider the case of $m_\sigma \neq 0$. Assume that the field configuration **s** interpolates between two degenerate ground states, so that $s_z = -1$ for $z \to -\infty$ and $s_z = 1$ for $z \to \infty$. Then, we can have a domain wall between the two ground states. For such a configuration, we obtain the BPS bound of the energy as

$$\begin{aligned} E &= \int dz \frac{\partial_z u \partial_z u^* + m_\sigma^2 |u|^2}{(1+|u|^2)^2} \\ &= \int dz \left[\frac{|\partial_z u + m_\sigma u|^2}{(1+|u|^2)^2} - \frac{m_\sigma (u^* \partial_z u + u \partial_z u^*)}{(1+|u|^2)^2} \right]. \end{aligned} \tag{31}$$

Here the second term corresponds to the charge of the domain wall as

$$\begin{aligned} T_{\rm w} &= -m_\sigma \int_{-\infty}^{+\infty} dz \frac{(u^* \partial_z u + u \partial_z u^*)}{(1+|u|^2)^2} \\ &= \frac{m_\sigma}{2} \int_{-\infty}^{+\infty} dz \partial_z s_z = \frac{m_\sigma}{2} [s_z]_{z=-\infty}^{z=+\infty}. \end{aligned} \tag{32}$$

Under the above boundary condition, the charge becomes $T_{\rm w} = +m_\sigma$. The energy is bounded by the domain wall charge $E \geqslant T_{\rm w}$, and the saturated solution satisfies the Bogomol'nyi equation

$$\partial_z u + m_\sigma u = 0. \tag{33}$$

Then we can obtain the BPS wall (kink) solutions

$$u_{\rm w} = e^{-m_\sigma (z-z_0) - i\phi_0}, \tag{34}$$

or, in terms of s_z, we have

$$s_z = \tanh[m_\sigma (z - z_0)]. \tag{35}$$

We can also consider the related solution with $T_{\rm w} = -m_\sigma$ [called the antiwall (antikink) solution], which is obtained by making the replacement $u \to u^{-1}$ ($s_z \to -s_z$). Here z_0 represents the position of the flat domain wall ($s_z = 0$) whose translation along the z axis causes the Nambu-Goldstone mode owing to breaking of the translational invariance. The phase $-\phi_0$ corresponds to the azimuthal angle of the pseudospin **s**, causing the breaking of the global U(1) symmetry *locally* along the wall. By promoting these two variables to dynamical fields as $z_0 \to z_0(x,y,t)$ and $\phi_0 \to \phi_0(x,y,t)$, we can construct an effective theory of the domain wall. In the relativistic context, the low-energy dynamics of a single domain in NLσM wall can be described by the Dirac-Born-Infeld (DBI) action [45,46], in which the *local* U(1) gauge fields on the wall are created by the dual transformation of the localized zero mode of the phase ϕ_0. This is an important foundation for the reason that the domain wall in NLσM can be identified as an analog of a D-brane [45,46,48].

C. Wall-vortex complexes: Analog D-brane solitons

By combining the above two solutions of the topological solitons, we can construct solutions in which vortices and domain walls coexist. For a fixed topological sector, namely, for vortices (a domain wall) parallel (perpendicular) to the z axis, the total energy [Eq. (24)] can be bounded with the topological charge as

$$E \geqslant |T_{\rm w}| + 2\pi |T_{\rm v}|. \tag{36}$$

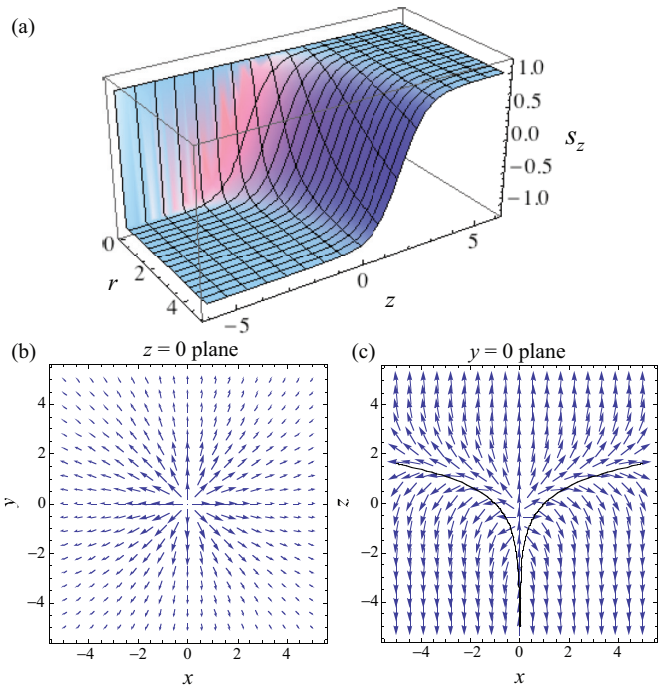

FIG. 4. (Color online) The simplest wall-vortex soliton, where a single vortex along the z axis for $z < 0$ is connected to the domain wall. The spin profile is given explicitly by Eq. (39), with $m_\sigma = 1$. (a) The profile of s_z. The spin texture of (b) the $z = 0$ plane and (c) the $y = 0$ plane. In (c), the wall position given by Eq. (40) is shown by a solid curve.

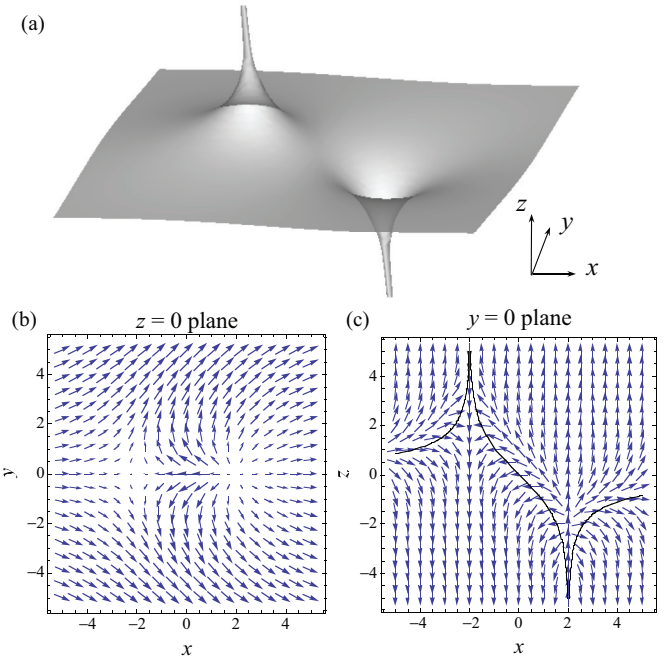

FIG. 5. (Color online) A wall-vortex soliton to which two vortices attach. (a) Isosurface of $s_z = 0$ for the solution [Eq. (41)] of NLσM. The corresponding spin textures $\mathbf{s}$ in the $z = 0$ plane and the $y = 0$ plane are shown in (b) and (c), respectively. In (c), the wall position given by Eq. (42) is shown by a solid curve. The wall becomes asymptotically flat as a result of the balance between the tensions of the attached vortices.

The BPS states can be represented in the form of separated coordinate variables [47],

$$u(\mathbf{r}) = u_{\rm v}(w)u_{\rm w}(z) = \frac{\prod_{i=1}^{N_n}\left(w - w_i^n\right)}{\prod_{i=1}^{N_s}\left(w - w_i^s\right)} e^{-m_\sigma(z-z_0)-i\phi_0}, \tag{37}$$

where $u_{\rm v}$ and $u_{\rm w}$ are satisfied with the Bogomol'nyi equations (29) and (33), and the forms of the solutions are given by Eq. (30) and Eq. (34), respectively.

To determine the properties of typical solutions, we plot the profile for the solutions of a single vortex and a single wall, expressed as

$$u(w,z) = e^{-m_\sigma z} w. \tag{38}$$

Here we choose $z_0 = 0$, $\phi_0 = 0$, $N_n = 1$, $N_s = 0$, and $w_1^n = 0$. This is the simplest composite wall-vortex solution. The corresponding spin profile is written as

$$\begin{pmatrix} s_x \\ s_y \\ s_z \end{pmatrix} = \begin{pmatrix} \frac{2xe^{-m_\sigma z}}{1+|w|^2e^{-2m_\sigma z}} \\ \frac{2ye^{-m_\sigma z}}{1+|w|^2e^{-2m_\sigma z}} \\ \frac{1-|w|^2e^{-2m_\sigma z}}{1+|w|^2e^{-2m_\sigma z}} \end{pmatrix}, \tag{39}$$

which is shown in Fig. 4. For a fixed $|w| = r$, we have a domain wall solution along the z direction but for a fixed z we have a vortex configuration in the x-y plane. For a fixed z, the coreless vortex has a scale size $\exp(m_\sigma z)$; thus, the size becomes infinity (zero) as $z \to +\infty$ ($z \to -\infty$). The wall position, i.e., the isosurface of $s_z = 0$, is described by a logarithmic function

$$z = \frac{1}{m_\sigma} \ln |w|, \tag{40}$$

as seen in Fig. 4(c). This situation is equivalent to the logarithmic bending when a membrane with a tension T is pulled by a pin at $r = 0$, where the profile of the membrane is given by $z = (\ln r)/T$ as a problem in mechanics. In the BPS solution, the tension of the domain wall is $T_{\rm w} = m_\sigma$ as shown above.

We can construct solutions in which an arbitrary number of vortices are connected to a domain wall, using Eq. (37), because of the absence of any static interaction between vortices. Figure 5 shows a solution in which two straight vortices along the z axis are connected to the wall on both sides. We assume that the vortices have ends at the positions $w = x_0$ and $-x_0$ on the wall. Then

$$u(w,z) = e^{-m_\sigma z}\frac{w - x_0}{w + x_0}. \tag{41}$$

The wall position is given by

$$z = \frac{1}{m_\sigma} \ln \left|\frac{w - x_0}{w + x_0}\right|, \tag{42}$$

which becomes asymptotically flat ($z \to 0$) for $|w| \to \infty$.

It is instructive here to understand schematically the wall configuration [Eqs. (40) and (42)] in terms of the tension of the vortices and walls. The wall bending can be interpreted to be caused by the tension of a vortex attached to the wall. For the case of Eq. (42), the tensional forces exerted by the two

vortices balance and the equilibrium position of the wall is well defined as $z = 0$ asymptotically. However, for Eq. (40), the position is ill defined since the force is unbalanced in the presence of a vortex only on one side of the wall. Similarly, the wall has an equilibrium position $z = z_0$ when the number of vortices on one side equals that on the other side, namely, $N_n = N_s$ in Eq. (37). The stiffness of the wall is represented by the coefficient m_σ^{-1} in Eqs. (40) and (42) with the wall tension $T_w = m_\sigma$. Therefore, the wall is more flexible as the wall tension m_σ decreases.

It should be mentioned here why this wall-vortex composite soliton has been referred to as a "D-brane" soliton in relativistic theory [45,46]. On a single D-brane, the Abelian gauge theory is realized. The present domain wall has a localized U(1) Nambu-Goldstone mode and it can be rewritten as the U(1) gauge field on the wall, which is a necessary degree of freedom for the DBI action of a D-brane. Gauntlett *et al.* [45] have shown that Eq. (37) reproduces the "BIon" solutions of the DBI action for D-branes in string theory by constructing an effective theory of the domain-wall world volume with collective coordinates $z_0(x,y,t)$ and $\phi_0(x,y,t)$ in $u_w(z)$, where ϕ_0 is periodically identified as $\phi_0 \to \phi_0 + 2\pi$. In the relativistic theory, the low-energy effective action for these collective coordinates is given by

$$I = -T_w \int d^3\xi \sqrt{-\det(G_{ij} + \partial_i\phi_0\partial_j\phi_0)}, \tag{43}$$

where $(\xi^0,\xi^1,\xi^2) = (t,x,y)$, and $G_{ij} = \eta_{ij} + \partial_i z_0 \partial_j z_0$ with $\eta_{ij} = \mathrm{diag}(-1,1,1)$ is the metric derived from the Minkowskii metric for a deformed membrane. Using the localized phase ϕ_0, we can introduce the U(1) gauge field A_j by taking a dual as

$$\partial_i\phi_0 = \epsilon_{ijk}\partial_j A_k. \tag{44}$$

The effective action of z_0 and A_i corresponds to the so-called DBI action of the D2-brane:

$$I = -T_w \int d^3\xi \sqrt{-\det(G_{ij} + F_{ij})}, \tag{45}$$

where $F_{ij} = \partial_i A_j - \partial_j A_i$ is the electromagnetic field strength. The solution from this effective theory in the background of a point source with an electric charge and a scalar charge is known as BIon, and its profile coincides precisely with that of the wall-vortex soliton in NLσM [45]. Thus, the end points of the vortex lines in NLσM can be seen as electrically charged particles within this effective theory [61,62], and the domain wall can be seen as a D-brane on which fundamental strings terminate. However, the correspondence needs to be modified in our nonrelativistic theory, which needs to be considered in further detail, although this is beyond the scope of the present paper.

IV. WALL-VORTEX COMPOSITE SOLITONS IN TWO-COMPONENT BECS

Mapping into NLσM can allow one to identify the domain wall of the two-component BECs as a nonrelativistic counterpart of the D-brane soliton. Based on the analytic solutions of topological solitons in the simplified NLσM, we next consider the structure of wall-vortex composite solitons in trapped two-component BECs. The generalized NLσM [Eq. (6)] has additional terms that are absent in the original NLσM. Here we discuss the modification of the soliton structure in the two-component BEC from the analytical solutions of Eq. (37).

For simplicity, we assume the symmetric parameters $m_1 = m_2 \equiv m$ and $g_{11} = g_{22} \equiv g = 4\pi\hbar^2 a/m$. We introduce the external trapping potential of Eq. (2). To nucleate and stabilize the vortices in trapped condensates, the system is supposed to be rotated at a rotation frequency $\mathbf{\Omega} = \Omega\hat{\mathbf{z}}$. To compare the numerical results with the previous analytical results directly, we introduce a length scale $\xi = \hbar/\sqrt{2mg\rho(0)}$ and an energy scale $\mu = g\rho(0)$, where $\rho(0)$ is the total density at the center of the trapping potential and can be estimated easily by applying the Thomas-Fermi approximation [4]. The coupled GP equation derived from the energy functional of Eq. (1) in the rotating frame of Ω can be written as

$$[-\nabla^2 + \tilde{V} + |\Psi_j|^2 + \gamma|\Psi_k|^2 - \alpha\tilde{\Omega}L_z]\Psi_j = \Psi_j, \tag{46}$$

where $\alpha = [4\pi\rho(0)aa_{\mathrm{ho}}^2]^{-1}$, with $a_{\mathrm{ho}} \equiv \sqrt{\hbar/m\omega}$ and $\gamma \equiv g_{12}/g$. The wave function has been scaled as $\Psi \to \sqrt{\rho(0)}\Psi$. In the following discussion, we confine ourselves to the parameter range $\gamma > 1$ for which phase separation occurs. The trapping potential $\tilde{V}$ can be written as

$$\tilde{V} = \frac{\alpha}{2}\left(\frac{\xi}{a_{\mathrm{ho}}}\right)^2 (r^2 + \lambda^2 z^2), \tag{47}$$

and the rotation frequency is $\tilde{\Omega} = \Omega/\omega_\perp$ The wave functions are normalized as $\int d\mathbf{r}|\Psi_j|^2 = N_j/[\xi^3\rho(0)]$. The numerical solutions given below are calculated by using the imaginary time propagation of Eq. (46).

We note that to realize the configuration shown in Fig. 1, the resulting domain wall should be perpendicular to the rotation axis. Then, it is desirable for the global shape of the condensate to be elongated along the rotation (z) axis, because such a configuration minimizes the interface area between the two domains to decrease the energy cost from surface tension. We thus prepare a cigar-shaped trap with $\lambda = 1/4$ to reduce the interface area and to keep the interface parallel in the x-y plane. As shown in Sec. IV C, however, the domain wall has a tendency to tilt from the x-y plane when there are vortices so as to reduce the gradient energy cost of the singular vortex cores. We fix the intraspecies s-wave scattering length as $a = 5.61$ nm and consider that the interspecies one, a_{12}, is a free parameter in the following. The use of the interspecies Feshbach resonance will be crucial for realizing such a situation experimentally [38].

A. Domain wall

We first discuss the structure of a domain wall in two-component BECs on the basis of the results of NLσM. Domain wall structures have been also studied by several authors [42,43]. The position of the domain wall is defined as a plane on which two components have the same amplitude $|\Psi_1| = |\Psi_2|$ ($s_z = 0$). Because the trapping potential does not play an essential role in the domain wall structure, we consider a homogeneous system with $\tilde{V} = 0$ as well as $\tilde{\Omega} = 0$. Then the system is characterized by only one parameter: $\gamma = g_{12}/g$.

Let us assume that the wall lies in the $z = 0$ plane and impose the following boundary conditions: $(\Psi_1,\Psi_2)^T \to$

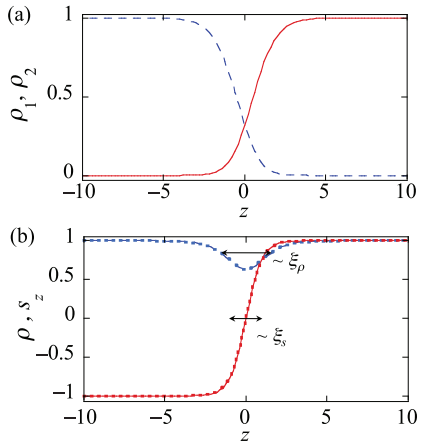

FIG. 6. (Color online) Numerical solutions of a domain wall in two-component BECs for $\gamma = 2$ with the boundary conditions $(\Psi_1,\Psi_2)^T \to (1,0)^T$ at $z \to +\infty$ and $(\Psi_1,\Psi_2)^T \to (0,1)^T$ at $z \to -\infty$. (a) Density profile of ρ_1 (solid curve) and ρ_2 (dashed curve). (b) Total density $\rho = \rho_1 + \rho_2$ (dashed curve) and the z component of the pseudospin s_z (solid curve). There are two characteristic length scales ξ_ρ and ξ_s in the solution. The results of the variational ansatz in Eqs. (53) and (54) for the profile of s_z and ρ are also plotted as dotted curves, where Δ_ρ in Eq. (54) is a variational parameter.

$(1,0)^T$ at $z \to +\infty$ and $(\Psi_1,\Psi_2)^T \to (0,1)^T$ at $z \to -\infty$. The typical profile of the domain wall solution is shown in Fig. 6. As z increases from negative to positive, the amplitude of Ψ_2 decreases as it approaches the domain wall, whereas that of Ψ_1 increases from zero with increasing distance from the domain wall. Representing the solution with total density $\rho = \rho_1 + \rho_2$ and the density difference, i.e., the z component of the pseudospin $s_z = (\rho_1 - \rho_2)/\rho$, clarifies that the domain wall is characterized by two different length scales, as shown in Fig. 6(b). The two length scales can be derived from the generalized NLσM [Eq. (19)], whose dimensionless form is given by

$$\tilde{E} = \int d\mathbf{r}\Big[(\nabla\sqrt{\tilde{\rho}})^2 + \frac{\tilde{\rho}}{4}\sum_\alpha(\nabla s_\alpha)^2 + \tilde{\rho}\tilde{v}_{\rm eff}^2 + \frac{1}{2}(\tilde{\rho}-1)^2 + \frac{1}{4}m_\sigma^2\tilde{\rho}^2\big(1-s_z^2\big)\Big]. \quad (48)$$

Here, we set $\tilde{\rho} = \rho/\rho(0)$ and $\tilde{\mathbf{v}}_{\rm eff} = (m\xi/\hbar)\mathbf{v}_{\rm eff}$; the tilde is omitted in the following discussion. By assuming that the system is uniform in x and y directions and $v_{\rm eff} = 0$, we consider the system spatially dependent only on the z direction. Using the identity

$$\sum_\alpha(\nabla s_\alpha)^2 = \frac{1}{1-s_z^2}[(\nabla s_z)^2 + (s_y\nabla s_x - s_x\nabla s_y)^2], \quad (49)$$

we can write the energy of the problem as

$$E_z = \int dz\Big[(\partial_z\sqrt{\rho})^2 + \frac{\rho}{4}\frac{(\partial_z s_z)^2}{1-s_z^2} + \frac{1}{2}(\rho-1)^2 + \frac{1}{4}m_\sigma^2\rho^2\big(1-s_z^2\big)\Big]. \quad (50)$$

The stationary solutions of the system satisfy the equations

$$-\frac{\partial_z^2\sqrt{\rho}}{\sqrt{\rho}} + \frac{1}{4}\frac{(\partial_z s_z)^2}{1-s_z^2} + \frac{1}{2}m_\sigma^2\rho\big(1-s_z^2\big) + \rho = 1, \quad (51)$$

$$\frac{\rho s_z(\partial_z s_z)^2}{\big(1-s_z^2\big)^2} + \frac{(\partial_z\rho)(\partial_z s_z) + \rho\big(\partial_z^2 s_z\big)}{1-s_z^2} + m_\sigma^2\rho^2 s_z = 0. \quad (52)$$

The asymptotic form of the profile can be obtained by linearizing with respect to ρ and s_z around the ground state value $\rho = 1$ and $s_z = \pm 1$ as $\rho \sim 1 - e^{\pm z/\xi_\rho} = 1 - e^{\pm\sqrt{2}z}$ and $s_z \sim \mp 1 \pm e^{\pm z/\xi_s} = \mp 1 \pm e^{\pm\sqrt{2}m_\sigma z}$ for $z \to \mp\infty$. This gives the characteristic length scales $\xi_\rho = 1/\sqrt{2}$ and $\xi_s = 1/(\sqrt{2}m_\sigma)$ in units of ξ. A similar structure with two characteristic lengths can be seen also in the vortex solutions of two-component BECs [63]. In the strongly segregating limit $g_{12} \to \infty$, the domain wall is characterized by a single length scale ξ_ρ because ξ_s vanishes.

Generally, the domain wall solution in NLσM is written as Eq. (34). In terms of the condensate wave function, the domain wall solution can be written as $\Psi_1 = f_{1d}(z - z_0)e^{-i\phi_0/2}$ and $\Psi_2 = f_{2d}(z - z_0)e^{i\phi_0/2}$, where f_{jd} is a real function with wall center z_0 and phase ϕ_0, which can be identified as the relative phase between two components $\phi_0 = \phi = \theta_2 - \theta_1$. The fixing of z_0 is due to the breaking of translational invariance by the given wall solution, whereas ϕ_0 is due to the breaking of global U(1) *around the domain wall*, i.e., a narrow overlapping region of the two-component wave functions, and consequently there appears a U(1) Nambu-Goldstone mode localized around the wall. This feature satisfies a part of the requirement discussed in Secs. III B and III C that the domain wall in two-component BECs can be referred to as a D-brane soliton [44].

It is instructive to consider the analytical form of the domain wall solution. The domain wall in NLσM of Eq. (20) under the $g \to \infty$ ($\xi_\rho \to 0$) limit has a single characteristic length ξ_s, where the profile is given by Eq. (34) or (35). When the spatial gradient of ρ is small enough for $\gamma \gtrsim 1$, the profile of s_z in the generalized NLσM must follow that in NLσM. We find that the domain wall solutions in Fig. 6 also follow correctly this profile function with slightly modified mass m'_σ:

$$s_z = \tanh(m'_\sigma z). \quad (53)$$

We make a fit of the numerical solution to Eq. (53) to extract the fitting value of m'_σ, which is plotted as a function of γ in Fig. 7(a). The mass parameter is almost in agreement with the values given in Eq. (21) in the σ model limit, although it begins to slightly deviate as γ increases. Thus, the domain wall in two-component BECs can be regarded as the same solitonic object in the original NLσM, including the quantitative details of the structure.

The remaining total density can be described by the ansatz

$$\rho = 1 - \Delta_\rho\,\mathrm{sech}\left(\frac{z}{\sqrt{2}\xi_\rho}\right), \quad (54)$$

where Δ_ρ is a variational parameter. According to Fig. 7(a), it is reasonable to put $m'_\sigma \approx m_\sigma$ in Eq. (53) as $s_z = \tanh(m_\sigma z) = \tanh(z/\sqrt{2}\xi_s)$; in other words, s_z is assumed to be given by Eq. (35) with $z_0 = 0$. Inserting Eqs. (35) and (54) into the energy of Eq. (50) and minimizing the energy with respect to Δ_ρ, we obtain the domain wall profile semianalytically as

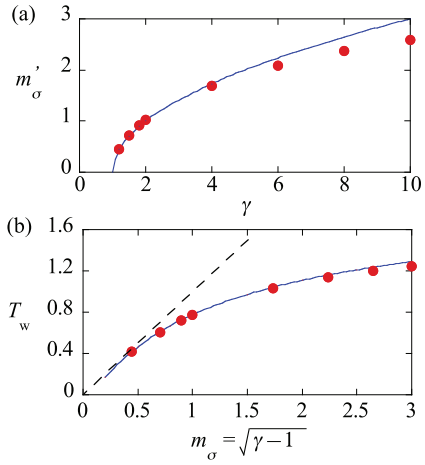

FIG. 7. (Color online) (a) The relation between m'_σ and γ. The circles are obtained by fitting Eq. (53) to the numerical solution with the fitting parameter m'_σ. We show the result for the σ-model limit $m_\sigma = \sqrt{|1-\gamma|}$ by the solid curve for comparison. (b) Tension of a domain wall as a function of $m_\sigma = \sqrt{|1-\gamma|}$. The solid curve represents the results calculated from the ansatz of Eqs. (35) and (54), where the energy is optimized with respect to the variational parameter Δ_ρ. The dots show the results calculated with numerical solutions. The dashed line represents the tension $T_w = m_\sigma$ in the σ-model limit.

shown in Fig. 6(b). The ansatz of Eqs. (35) and (54) agrees with the numerical result almost perfectly. This minimized energy per unit area [Eq. (50)] in the presence of a domain wall represents the tension of the wall, $T_w = E_z^{\min}$, which is an extended version of Eq. (32) for two-component BECs. The tension is simply given by $T_w = m_\sigma$ in the σ model case, whereas it is significantly reduced in the BEC case because of the additional contribution of the total density, as shown in Fig. 7(b).

B. Axisymmetric structure of wall-vortex complex

We next consider an axisymmetric wall-vortex soliton in trapped two-component BECs. As shown in Fig. 1, the Ψ_1 (Ψ_2) domain is placed at $z > 0$ ($z < 0$) and each component is assumed to have a straight vortex line at the center. The axisymmetric solution $\Psi_j = f_j(r,z)e^{in_j\theta}$ with real function f_j, polar angle θ, and vortex winding number n_j can be obtained by numerically solving the coupled GP equations,

$$\left[-\left(\frac{\partial^2}{\partial r^2} + \frac{1}{r}\frac{\partial}{\partial r} + \frac{\partial^2}{\partial z^2} - \frac{n_j}{r^2}\right) + \tilde{V} + f_j^2 + \gamma f_k^2\right] f_j = f_j. \tag{55}$$

The parameters are the ratio of the coupling constants, $\gamma \equiv g_{12}/g$, and the winding number, n_j. Here we assume for simplicity that both components have the same particle number N, and we set $m = m_{^{87}\mathrm{Rb}}$, $\omega = 20 \times 2\pi$ Hz, and $N = 10^5$.

Before proceeding, we present some notes on the numerical solutions. In the energy-minimization process of the numerical simulations, the chemical potential is usually fixed in a homogeneous problem without a trapping potential, so that the particle number of each component is not conserved. Thus, the pressure difference between two components, originating

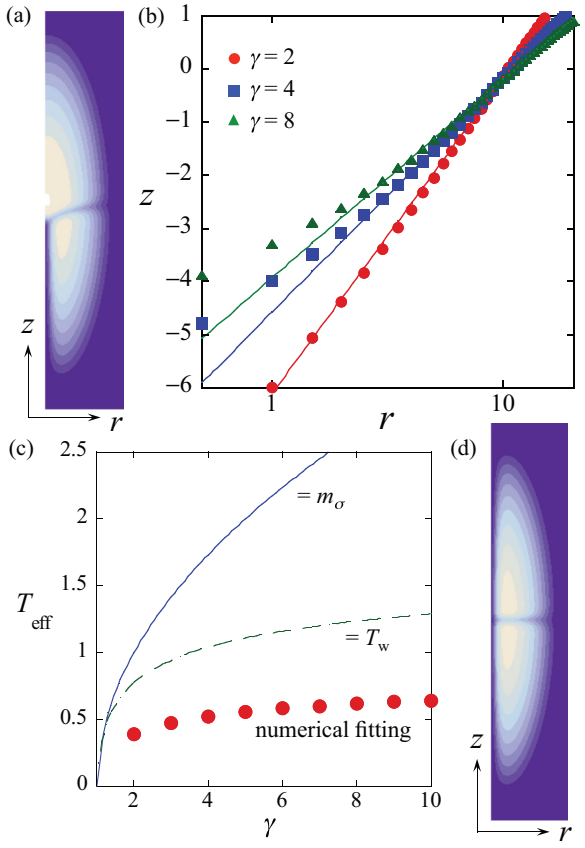

FIG. 8. (Color online) Numerical solutions of the axisymmetric wall-vortex soliton obtained by the GP equation. (a) Profile of the total density for $(n_1,n_2) = (0,1)$ and $\gamma = 2$. (b) Semilog plot of the wall position for several values of $\gamma = g_{12}/g$. Each plot can be fitted by the logarithmic function $z = A \ln r + B$, with $A = 2.59$, 1.91, and 1.62 for $\gamma = 2$, 4, and 8, respectively, where the fitting is made by using the data for $r > 5$ to avoid the contribution of the singular vortex core. (c) Effective tension determined from the relation $T_{\mathrm{eff}} = A^{-1}$ [see Eq. (57)] as a function of γ. The circles are obtained from the numerical fitting. The solid curve corresponds to the σ-model limit: $T_{\mathrm{eff}} = m_\sigma = \sqrt{|1-\gamma|}$; the dashed curve is the domain wall tension obtained by the variational approach, shown as the solid curve in Fig. 7(b). (d) Profile of the total density for $(n_1,n_2) = (1,1)$.

from the asymmetry of the solution, leads to a decrease in the population of the energetically unfavorable vortical component during the imaginary time evolution. Eventually, the vortex-free component fills all space as a final equilibrium solution. To obtain the desired solution, we have to adjust the chemical potential difference to balance the pressure between the two components, which is a troublesome task. Thus, we perform the numerical minimization by fixing the particle number in each component in the presence of the trapping potential, which is an experimentally relevant situation.

Figures 8(a) and 8(b) show the profile of the total density $\rho = \rho_1 + \rho_2$ for $\gamma = 2$ and the positions of the domain wall, namely, $s_z = 0$ ($|\Psi_1| = |\Psi_2|$), for several values of γ, respectively. The vortex in the Ψ_2 component near the domain wall forms a coreless vortex, whose core is filled by the density of the Ψ_1 component and transforms into a singular vortex with distance from the domain wall. Thus, the total density

ρ is reduced at the position of the domain wall and vanishes at the singular vortex core around $r = 0$ with a z that is less than some finite negative value. The appearance of the singular core can be understood from the generalized NLσM. When we consider the phases $\theta_1 = 0$ and $\theta_2 = \theta$ for the case of Fig. 8(a), for example, we obtain

$$\tilde{v}_{\rm eff}^2 = \frac{1}{4}(\nabla\theta_2)^2(1-s_z)^2 = \frac{1}{4r^2}(1-s_z)^2. \tag{56}$$

This kinetic energy density vanishes in the Ψ_1 ($s_z = 1$) domain, whereas it contributes to the energy as $\tilde{\rho} r^{-2}$ in the Ψ_2 ($s_z = -1$) domain. The latter divergent contribution makes a singular vortex core in the Ψ_2 component around $r = 0$.

This inhomogeneity of ρ implies that the assumption of uniform total density that is used to derive NLσM in Eq. (20) is not valid and the solution is expected to deviate from Eq. (38). Nevertheless, the spin texture of this solution is almost identical to that in Fig. 4. The plot of the wall position in Fig. 8(b) can be well fitted by the logarithmic function $z = A \ln r + B$, as expected from Eq. (40). Here, the offset B is introduced owing to the deviation of the domain wall position from a pure logarithmic function of r with no offset, because of the presence of the vortex core. Thus, the qualitative structural feature of the wall-vortex composite soliton in two-component BECs is not changed from the BPS solutions of NLσM. According to Eq. (40), we apply an analogy of a pulled membrane to this situation and extract the effective tension $T_{\rm eff}$ of the domain wall from the numerical fitting with the relation

$$z - B = \frac{1}{T_{\rm eff}} \ln r. \tag{57}$$

This fitting function does not account for the presence of the velocity field $\mathbf{v}_{\rm eff}$. As shown in Fig. 8(c), the value of the effective tension $T_{\rm eff} = A^{-1}$ is significantly reduced from not only $T_{\rm w} = m_\sigma = \sqrt{|1-\gamma|}$ of Eq. (20) in the σ model limit but also $T_{\rm w}$ of the BEC domain wall in Fig. 7(b). This means that the domain wall in this composite soliton can be more flexible than that in a single domain wall. This further reduction of the tension may be attributable to the following effects. (i) The rotational flow of a vortex causes the density inhomogeneity, where the density changes as $\rho_2 \sim r^2/(2+r^2)$ around the singular vortex core. The density difference between ρ_1 and ρ_2 ($\rho_1 > \rho_2$ near the wall) can enhance pressure from Ψ_1 to Ψ_2 and lead to more flexible bending of the wall. (ii) The trapping potential also gives rise to a density inhomogeneity, and the pressure balance can be modified radially. Contribution (ii) is probably minor because Fig. 8(b) shows that the wall is well fitted logarithmically even for a large r [64].

Figure 8(d) shows the profile of the total density for $(n_1,n_2) = (1,1)$. Because of the balance of the vortex tension, the domain wall becomes flat. This situation corresponds to $x_0 = 0$ in Eq. (41) in the σ model. There are two singular vortices that have infinitely thin distribution (δ-functional form) of vorticity; thus, we have only the domain wall structure because the relative phase between the two components is uniform everywhere.

Figure 9 shows the solution for $(n_1,n_2) = (0,2)$ and $(n_1,n_2) = (0,3)$. In these cases, the size of the vortex core extends radially, and the core is filled by the Ψ_1 component to be identified as the coreless vortex. According to the BPS

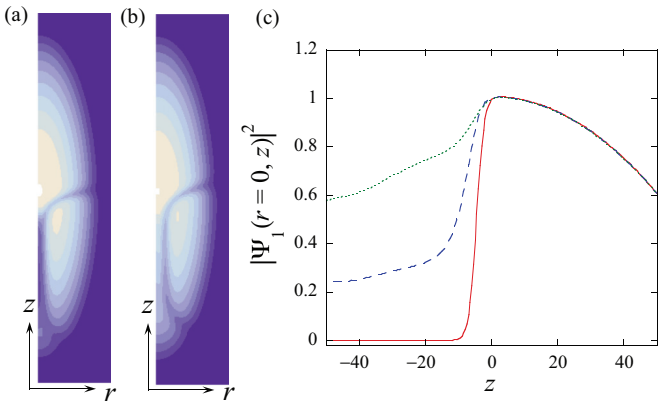

FIG. 9. (Color online) Numerical solutions of the axisymmetric wall-vortex soliton obtained by the GP equation for $\gamma = 2$. Profiles of the total density for (a) $(n_1,n_2) = (0,2)$ and (b) $(n_1,n_2) = (0,3)$. (c) Profile of ρ_1 at $r = 0$ as a function of z for $n_2 = 1$ (solid curve), 2 (dashed curve), and 3 (dotted curve).

solution of NLσM, $u(w,z) = e^{-m_\sigma z} w^{n_2}$, the position of the domain wall is expected to become

$$z - B \simeq \frac{n_2}{T_{\rm eff}} \ln r. \tag{58}$$

A logarithmic fitting $z = A \ln r + B$ (for $r > 5$) of these solutions gives A =2.59, 4.44, and 6.20 for $n_2 = 1$, 2, and 3, respectively. This is in good agreement with the NLσM solution but its increase is lower than the expected linear dependence. This also means that the tensile force for a domain wall pulled by a multiply quantized vortex in BECs is weaker than that of a multiply quantized BPS vortex.

Note that, in the case with $n_2 > 1$ in Fig. 9, the total density does not vanish at the vortex core, as seen in Fig. 9(c). Since the core size of the multiply quantized vortex becomes large with increasing n_2, for example, $\sim[r^2/(2+r^2)]^{n_2}$, the density of the vortex-free component can enter the core easily. However, the vortex core for $n_2 = 1$ is apparently singular without density. This indicates that there is a critical core size that allows the filling of the density inside the core. From different points of view, there is a critical ratio of the chemical potential $(\mu_2/\mu_1)_c$ that determines whether the vortex core can be filled with the other nonvortex component for a given γ [66]. The 2D simulation shows that the optimized $(n_1,n_2) = (0,1)$ vortex state for $\mu_1 = \mu_2 = 1$ and $\gamma = 2$ is actually characterized by an empty vortex core.

C. Nonaxisymmetric structure: A wall with multiple vortices

Next, we remove the axisymmetric condition and calculate the equilibrium state by using the imaginary time propagation of Eq. (46) in full 3D space from a suitably prepared initial configuration. To realize the final equilibrium configuration as shown in Fig. 1, we prepare the phase-separated state in which Ψ_1 (Ψ_2) domains with some phase singularities (seeds of vortices) are located in the $z > 0$ (<0) region as the initial state of the calculation.

The panels of Fig. 10 show the 3D distributions of the density difference $|\rho_1 - \rho_2| \propto |s_z|$ of the equilibrium state for several Ω values; this presentation is suitable for

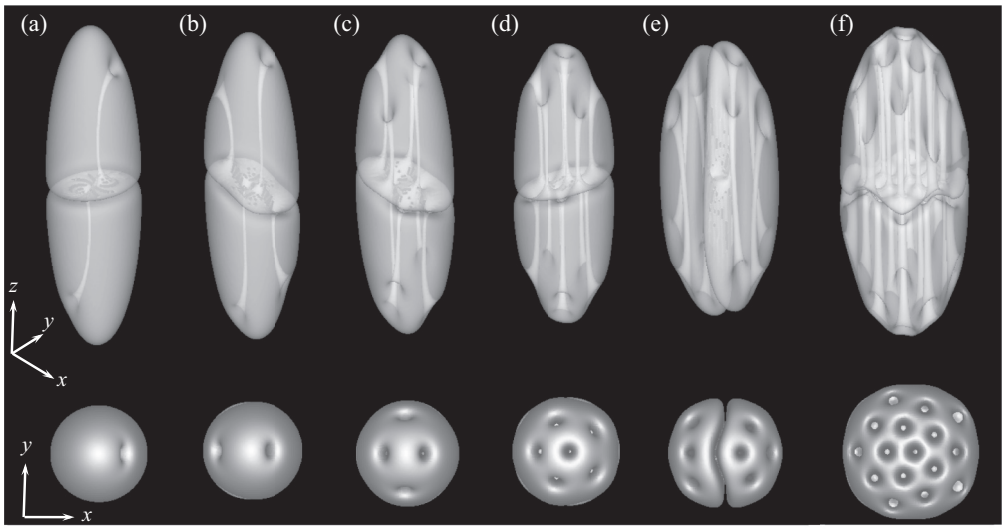

FIG. 10. Configuration of a wall connecting multiple vortices in trapped BECs. The panels show the profile of the density difference $|\rho_1 - \rho_2| \propto |s_z|$ (isosurface of $|\rho_1 - \rho_2| = 0.0005$) for $\tilde{\Omega} =$ (a) 0.4, (b) 0.5, (c) 0.6, (d) 0.7, and (e) 0.8. The parameter values used are $\lambda = 1/4$, $N = 5.5 \times 10^4$, and $a_{12} = 2a$. The bottom panels show the top view of the top panels. In (f), we show the equilibrium structure for $\tilde{\Omega} = 0.8$, $\lambda = 1/4$, and $a_{12} = 2a$ but the particle number $N = 1.65 \times 10^5$, which is three times as that in (e).

visualizing the region of the vortex core and the domain wall (surface of $\rho_1 = \rho_2$). This configuration is energetically stable since it is obtained by imaginary time propagation. For $\tilde{\Omega} = 0.40$, we obtain the $(n_1,n_2) = (1,1)$ state. In contrast to the axisymmetric structure of Fig. 8(c), the end point of the vortices in each component is spontaneously displaced from the center, corresponding to $x_0 \neq 0$ in Eq. (41). Although the energy is independent of x_0 in the BPS solution of NLσM, this displacement results from the fact that the vorticity should be distributed broadly near the domain wall so as to reduce the associated kinetic energy as well as to reduce the gradient of ρ. Further, the vortex line is slightly bent because of the elongated trapping potential [67]. Because our calculation uses the same rotation frequency $\tilde{\Omega}$ for both components, the number of nucleating vortices should be the same for both components [68].

When the rotation is further increased, multiple vortices form a lattice in each component. Then, the domain wall begins to incline from the $z = 0$ plane [Figs. 10(b)–10(d)] and eventually becomes parallel to the rotation axis [Fig. 10(e)], even though the interface area (energy) increases. This is a vortex sheet structure [53]. The reason that this vortex sheet structure is preferred is because the absorption of the vortices into the domain wall leads to a decrease in the gradient energy of the singular vortex cores. This effect is also absent in the composite solitons of NLσM, which is free from the density gradient energy. Actually, in the Thomas-Fermi limit, the gradient energy of the vortex core decreases, so that the structure such as that depicted in Fig. 1 is expected to persist. The example is shown in Fig. 10(f), where the particle number is three times larger than that of Fig. 10(e). In this parameter setting, the domain wall is nearly parallel to the $z = 0$ plane.

Another interesting property of this system at high rotation frequencies is that an ordering structure of many interface defects can emerge owing to the complicated interactions. In each domain far from the domain wall, singular vortices form an Abrikosov triangular lattice. However, singular vortices become coreless vortices near the domain wall and a lattice of 2D skyrmions forms on the domain wall. A typical example is shown in Fig. 11. It is important to note that $\rho_1 = \rho_2$ on the domain wall, and a miscible state is effectively realized in this restricted 2D system of immiscible condensates. This effective 2D system can be characterized by the effective 2D coupling constant $g_{12}^{\rm eff}$, which determines the lattice structure of the 2D skyrmions on the domain wall but is not straightforwardly related to the fundamental coupling constant g_{12} of the full 3D system. We note that 2D skyrmions tend to form a square lattice rather than a triangular one [69]. In the parameter setting used for Fig. 11, the vortex end points are shifted relative to each other on the domain wall to form a rectangular lattice of 2D skyrmions. With increasing g_{12}, we can see, by comparing panels (a) and (b), that the tendency to form a rectangular lattice from a triangular lattice becomes noticeable. These features are consistent with the phase diagram of a vortex lattice in 2D miscible two-component BECs [50,52,69], and they may originate from the static vortex-vortex interaction [70], which is absent in the BPS solution. In Fig. 11(b), our numerical solutions show that the domain wall tends to be inclined from the $z = 0$ plane such that shorter sides of the rectangles of the vortex lattice elongate. This tendency may be explained by competition between the contributions to the total energy from the wall and the vortices in trapping systems. To ensure the energetics, we need to perform numerical simulations using a much larger system size, which we plan to attempt in a future work.

V. DISCUSSION AND CONCLUSION

We have shown that a wall-vortex composite soliton, referred to as a D-brane soliton in field theoretical models, can be realized as an energetically stable solitonic object in phase-separated rotating two-component BECs. Based on the NLσM derived from the two-component GP model, we obtain the analytic solution of the topological solitons, including

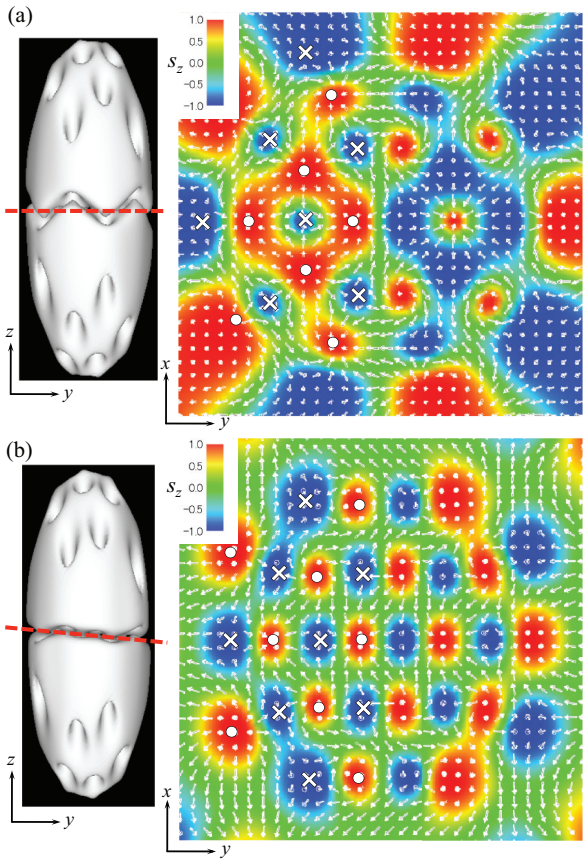

FIG. 11. (Color online) Equilibrium structure and spin texture along the $\langle s_z \rangle = 0$ plane for $\tilde{\Omega} = 0.8$, $\lambda = 1/4$, $N = 1.65 \times 10^5$, and (a) $a_{12} = 2a$ and (b) $a_{12} = 4a$; the parameters in (a) are the same as those of Fig. 10(f). Left panels show the isosurface of the density difference $|\rho_1 - \rho_2|$ as in Fig. 10. Right panels show the distribution of the pseudospin field $\mathbf{s}(\mathbf{r})$ in the plane (a) along the $z = 0$ plane and (b) slightly declined from the $z = 0$ plane, indicated by the bold lines in the left panels. The color scale shows the magnitude of s_z. The circles and crosses mark the position of Ψ_2 and Ψ_1 vortices, respectively, where we only mark those in the $y < 0$ region for clarity.

domain walls, vortices, and their complexes, by taking the BPS bound of the total energy, which is a widely used technique in field theory [1]. The topological solitons in trapped BECs are found to have almost the same character as the BPS saturated solution in NLσM. The inhomogeneity of the total density modifies the profile of the soliton quantitatively through the reduction of the domain wall tension. The domain wall pulled by a vortex is logarithmically bent as the BPS wall in NLσM, but it bends more flexibly than expected by the tension of the BEC domain wall. Numerical analysis of full 3D simulations reveals that the complicated energetic constraint influences the determination of the equilibrium configuration, affecting the surface tension of the wall, the gradient energy of the density, and the interactions between vortices and those between interface defects. This raises the problem of how the properties of an effective 2D system realized in an interface of multicomponent condensates can be considered, which can be affected by extra dimensions (bulk regions).

It should be noted, however, that there is one significant difference between the wall-vortex composite soliton in BECs and that in NLσM. In the BECs described by the GP model, the total density vanishes in the singular vortex core for $n_2 = 1$ because the density of the nonrotating component does not enter into the vortex core, as seen in Fig. 9(c). The coreless vortex near the domain wall shrinks to a singular vortex over a finite distance and thus we can identify a point connecting a singular vortex and a coreless vortex. This is in contrast to the case in NLσM, where a coreless vortex extends to infinity along the thin vortex core avoiding the singularity, since $\mathbf{s}$ is well defined everywhere. Hence, a connecting point is absent in the wall-vortex soliton. In a field theoretical model, the connecting point forms a defect called a "boojum," which provides the negative binding energy of vortices and a wall and half of the negative charge of a single monopole [47,48]. Boojums are known as point defects existing on the surface of the ordered phase; the name was first introduced to physics by Mermin in the context of superfluid ^{3}He [71]. Boojums can exist in different physical systems, such as the interface separating the A and B phases of superfluid ^{3}He [8,72], liquid crystals [73], the Langmuir monolayers at air-water interfaces [74], multicomponent BECs with a spatially tuned interspecies interaction [75,76], and high-density quark matter [77]. In the present model, boojums can be found at the end points of vortices on the domain wall, at which the vortices change their type from singular to coreless. A suitable topological charge for boojums in two-component BECs can be derived by noting the analogy with Abelian gauge theory [65]. A detailed study of the distribution of the boojum charge and the interactions between boojums remains to be investigated in a future study.

As pointed out in Ref. [44], domain walls in two-component BECs are useful for simulating some analogous phenomena of the D-brane physics in a laboratory. One famous example is a nonequilibrium dynamics such as brane-antibrane annihilation, which was proposed as a possible explanation for the inflationary universe in string theory. In brane-world scenarios of cosmic inflation, the annihilation may lead to defect production that could be directly observed in atomic BECs; the experiment has been performed with superfluid ^{3}He A-B interfaces, but the detection of defects is difficult [78]. Recently, we proposed that domain-wall annihilation in two-component BECs actually demonstrates a brane-antibrane collision and a subsequent creation of cosmic strings, causing tachyon condensation accompanied by spontaneous Z_2 symmetry breaking in a 2D subspace [79]. We have also proposed that, when strings are stretched between the brane and the antibrane, namely, when the filling component has vortices perpendicular to the wall, "cosmic vortons" can emerge via a similar instability [29]. We hope that our work motivates experimentalists to create composite solitons and study their real-time evolution.

ACKNOWLEDGMENTS

This work was supported by KAKENHI from JSPS (Grants No. 21340104, No. 21740267, and No. 23740198). This work was also supported by the "Topological Quantum Phenomena" Grant-in Aid (Grants No. 22103003 and No. 23103515) for Scientific Research on Innovative Areas from the Ministry of Education, Culture, Sports, Science, and Technology (MEXT) of Japan.

[1] N. Manton and P. Sutcliffe, *Topological Solitons* (Cambridge University Press, Cambridge, UK, 2004).

[2] R. J. Donnelly, *Quantized Vortices in Helium II* (Cambridge University Press, Cambridge, UK, 1991).

[3] T. W. B. Kibble, J. Phys. A **9**, 1387 (1976).

[4] C. J. Pethick and H. Smith, *Bose-Einstein Condensation in Dilute Gases*, 2nd ed. (Cambridge University Press, Cambridge, UK, 2008).

[5] D. J. Frantzeskakis, J. Phys. A: Math. Theor. **43**, 213001 (2010).

[6] A. Fetter, Rev. Mod. Phys. **81**, 647 (2009); K. Kasamatsu and M. Tsubota, in *Progress in Low Temperature Physics*, edited by W. P. Halperin and M. Tsubota (Elsevier, Amsterdam, 2009), Vol. 16, p. 351.

[7] Y. Kawaguchi and M. Ueda, Phys. Rep. **520**, 253 (2012).

[8] G. E. Volovik, *The Universe in a Helium Droplet* (Clarendon Press, Oxford, UK, 2003).

[9] C. Becker, S. Stellmer, P. Soltan-Panahi, S. Dörscher, M. Baumert, E.-M. Richter, J. Kronjäger, K. Bongs, and K. Sengstock, Nat. Phys. **4**, 496 (2008).

[10] C. Hamner, J. J. Chang, P. Engels, and M. A. Hoefer, Phys. Rev. Lett. **106**, 065302 (2011).

[11] Th. Busch and J. R. Anglin, Phys. Rev. Lett. **87**, 010401 (2001).

[12] M. R. Matthews, B. P. Anderson, P. C. Haljan, D. S. Hall, C. E. Wieman, and E. A. Cornell, Phys. Rev. Lett. **83**, 2498 (1999).

[13] A. E. Leanhardt, Y. Shin, D. Kielpinski, D. E. Pritchard, and W. Ketterle, Phys. Rev. Lett. **90**, 140403 (2003).

[14] V. Schweikhard, I. Coddington, P. Engels, S. Tung, and E. A. Cornell, Phys. Rev. Lett. **93**, 210403 (2004).

[15] L. S. Leslie, A. Hansen, K. C. Wright, B. M. Deutsch, and N. P. Bigelow, Phys. Rev. Lett. **103**, 250401 (2009).

[16] J. Y. Choi, W. J. Kwon, and Y. I. Shin, Phys. Rev. Lett. **108**, 035301 (2012).

[17] H. T. C. Stoof, E. Vliegen, and U. Al Khawaja, Phys. Rev. Lett. **87**, 120407 (2001).

[18] J.-P. Martikainen, A. Collin, and K.-A. Suominen, Phys. Rev. Lett. **88**, 090404 (2002).

[19] C. M. Savage and J. Ruostekoski, Phys. Rev. A **68**, 043604 (2003).

[20] J. Ruostekoski and J. R. Anglin, Phys. Rev. Lett. **91**, 190402 (2003).

[21] V. Pietilä and M. Möttönen, Phys. Rev. Lett. **102**, 080403 (2009); **103**, 030401 (2009); E. Ruokokoski, V. Pietilä, and M. Möttönen, Phys. Rev. A **84**, 063627 (2011).

[22] U. Al Khawaja and H. T. C. Stoof, Nature (London) **411**, 918 (2001).

[23] J. Ruostekoski and J. R. Anglin, Phys. Rev. Lett. **86**, 3934 (2001).

[24] R. A. Battye, N. R. Cooper, and P. M. Sutcliffe, Phys. Rev. Lett. **88**, 080401 (2002).

[25] C. M. Savage and J. Ruostekoski, Phys. Rev. Lett. **91**, 010403 (2003); J. Ruostekoski, Phys. Rev. A **70**, 041601(R) (2004).

[26] I. F. Herbut and M. Oshikawa, Phys. Rev. Lett. **97**, 080403 (2006); A. Tokuno, Y. Mitamura, M. Oshikawa, and I. F. Herbut, Phys. Rev. A **79**, 053626 (2009).

[27] T. Kawakami, T. Mizushima, M. Nitta, and K. Machida, Phys. Rev. Lett. **109**, 015301 (2012).

[28] M. A. Metlitski and A. R. Zhitnitsky, J. High Energy Phys. 06 (2004) 017.

[29] M. Nitta, K. Kasamatsu, M. Tsubota, and H. Takeuchi, Phys. Rev. A **85**, 053639 (2012).

[30] Y. M. Cho, H. Khim, and P. Zhang, Phys. Rev. A **72**, 063603 (2005).

[31] Y. Kawaguchi, M. Nitta, and M. Ueda, Phys. Rev. Lett. **100**, 180403 (2008).

[32] C. J. Myatt, E. A. Burt, R. W. Ghrist, E. A. Cornell, and C. E. Wieman, Phys. Rev. Lett. **78**, 586 (1997).

[33] D. S. Hall, M. R. Matthews, J. R. Ensher, C. E. Wieman, and E. A. Cornell, Phys. Rev. Lett. **81**, 1539 (1998).

[34] K. M. Mertes, J. W. Merrill, R. Carretero-González, D. J. Frantzeskakis, P. G. Kevrekidis, and D. S. Hall, Phys. Rev. Lett. **99**, 190402 (2007).

[35] S. Tojo, Y. Taguchi, Y. Masuyama, T. Hayashi, H. Saito, and T. Hirano, Phys. Rev. A **82**, 033609 (2010).

[36] G. Modugno, M. Modugno, F. Riboli, G. Roati, and M. Inguscio, Phys. Rev. Lett. **89**, 190404 (2002).

[37] G. Thalhammer, G. Barontini, L. De Sarlo, J. Catani, F. Minardi, and M. Inguscio, Phys. Rev. Lett. **100**, 210402 (2008).

[38] S. B. Papp, J. M. Pino, and C. E. Wieman, Phys. Rev. Lett. **101**, 040402 (2008).

[39] D. J. McCarron, H. W. Cho, D. L. Jenkin, M. P. Köppinger, and S. L. Cornish, Phys. Rev. A **84**, 011603(R) (2011).

[40] E. Timmermans, Phys. Rev. Lett. **81**, 5718 (1998).

[41] P. Ao and S. T. Chui, Phys. Rev. A **58**, 4836 (1998).

[42] S. Coen and M. Haelterman, Phys. Rev. Lett. **87**, 140401 (2001).

[43] R. A. Barankov, Phys. Rev. A **66**, 013612 (2002); B. Van Schaeybroeck, *ibid.* **78**, 023624 (2008).

[44] K. Kasamatsu, H. Takeuchi, M. Nitta, and M. Tsubota, J. High Energy Phys. 11 (2010) 068.

[45] J. P. Gauntlett, R. Portugues, D. Tong, and P. K. Townsend, Phys. Rev. D **63**, 085002 (2001).

[46] M. Shifman and A. Yung, Phys. Rev. D **67**, 125007 (2003).

[47] Y. Isozumi, M. Nitta, K. Ohashi, and N. Sakai, Phys. Rev. D **71**, 065018 (2005).

[48] N. Sakai and D. Tong, J. High Energy Phys. 03 (2005) 019; D. Tong, *ibid.* 02 (2006) 030; R. Auzzi, M. Shifman, and A. Yung, Phys. Rev. D **72**, 025002 (2005).

[49] In field theoretical models, all possible composite solitons of domain walls, vortices, monopoles, and instantons, including D-brane solitons, were reviewed by M. Eto, Y. Isozumi, M. Nitta, K. Ohashi, and N. Sakai, J. Phys. A **39**, R315 (2006), and M. Eto, Y. Isozumi, M. Nitta, and K. Ohashi, Nucl. Phys. B **752**, 140 (2006).

[50] K. Kasamatsu, M. Tsubota, and M. Ueda, Int. J. Mod. Phys. **19**, 1835 (2005).

[51] K. Kasamatsu, M. Tsubota, and M. Ueda, Phys. Rev. A **71**, 043611 (2005).

[52] P. Mason and A. Aftalion, Phys. Rev. A **84**, 033611 (2011).

[53] K. Kasamatsu and M. Tsubota, Phys. Rev. A **79**, 023606 (2009).

[54] E. Babaev, L. D. Faddeev, and A. J. Niemi, Phys. Rev. B **65**, 100512(R) (2002).

[55] Y. Lin, R. L. Compton, K. J. Garcia, J. V. Porto, and I. B. Spielman, Nature (London) **462**, 628 (2009).

[56] This simplification could be verified under either of the following situations. (i) When there are many vortices in the system, the condensates could mimic the rigid-body rotation as $\boldsymbol{v}_g + \boldsymbol{v}_s \sim \boldsymbol{\Omega} \times \mathbf{r}$. (ii) If $\mathbf{A}$ is an artificial vector potential, it can be tuned spatially to cancel the contribution of $\boldsymbol{v}_g + \boldsymbol{v}_s$.

[57] E. B. Bogomol'nyi, Yad. Fiz. **24**, 861 (1976) [Sov. J. Nucl. Phys. **24**, 449 (1976)].
[58] M. Prasad and C. M. Sommerfield, Phys. Rev. Lett. **35**, 760 (1975).
[59] A. A. Belavin and A. M. Polyakov, Pis'ma Zh. Eksp. Teor. Fiz. **22**, 503 (1975) [JETP Lett. **22**, 245 (1975)].
[60] P. W. Anderson and G. Toulouse, Phys. Rev. Lett. **38**, 508 (1977).
[61] G. W. Gibbons, Nucl. Phys. B **514**, 603 (1998).
[62] C. G. Callan and J. M. Maldacena, Nucl. Phys. B **513**, 198 (1998).
[63] M. Eto, K. Kasamatsu, M. Nitta, H. Takeuchi, and M. Tsubota, Phys. Rev. A **83**, 063603 (2011).
[64] In Ref. [65], we calculate the stationary solution of the domain wall attached by a vortex in a uniform system through a fine tuning of the chemical potentials μ_1 and μ_2 (Fig. 9 in Ref. [65]). The numerical fitting shows that the effective tension of the domain wall in a uniform system is almost equal to that obtained in the trapped system.
[65] K. Kasamatsu, H. Takeuchi, and M. Nitta, arXiv:1303.4469 [J. Phys.: Condens. Matter (to be published)].
[66] S. Hayashi, M. Tsubota, and H. Takeuchi, Phys. Rev. A **87**, 063628 (2013).
[67] J. J. García-Ripoll and V. M. Pérez-García, Phys. Rev. A **63**, 041603(R) (2001).
[68] Even in the present scheme, where the same rotation is applied for both components, the stabilization of a vortex only in one component is possible if we choose the suitable asymmetric seed for two components in the initial condition because of the hysteresis effect [44,67]; the critical rotation frequency for vortex nucleation and that for vortex stabilization is generally different. Preparing vortices only in one component is more easy when there is an imbalance of the parameters for the Ψ_1 and Ψ_2 components.
[69] E. J. Mueller and T.-L. Ho, Phys. Rev. Lett. **88**, 180403 (2002); K. Kasamatsu, M. Tsubota, and M. Ueda, *ibid.* **91**, 150406 (2003).
[70] A. Aftalion, P. Mason, and J. Wei, Phys. Rev. A **85**, 033614 (2012).
[71] N. D. Mermin, in *Quantum Fluids and Solids*, edited by S. B. Trickey, E. D. Adams, and J. W. Dufty (Plenum, New York, 1977), p. 3.
[72] R. Blaauwgeers, V. B. Eltsov, G. Eska, A. P. Finne, R. P. Haley, M. Krusius, J. J. Ruohio, L. Skrbek, and G. E. Volovik, Phys. Rev. Lett. **89**, 155301 (2002).
[73] D. L. Stein, R. D. Pisarski, and P. W. Anderson, Phys. Rev. Lett. **40**, 1269 (1978); S. A. Langer and J. P. Sethna, Phys. Rev. A **34**, 5035 (1986); M. Kleman and O. D. Lavrentovich, *Soft Matter Physics: An Introduction* (Springer-Verlag, New York, 2003).
[74] T. M. Fischer, R. F. Bruinsma, and C. M. Knobler, Phys. Rev. E **50**, 413 (1994); S. Riviere and J. Meunier, Phys. Rev. Lett. **74**, 2495 (1995).
[75] H. Takeuchi and M. Tsubota, J. Phys. Soc. Jpn. **75**, 063601 (2006); K. Kasamatsu, H. Takeuchi, M. Nitta, and M. Tsubota, J. Low Temp. Phys. **158**, 99 (2010).
[76] M. O. Borgh and J. Ruostekoski, Phys. Rev. Lett. **109**, 015302 (2012); Phys. Rev. A **87**, 033617 (2013).
[77] M. Cipriani, W. Vinci, and M. Nitta, Phys. Rev. D **86**, 121704(R) (2012).
[78] D. I. Bradley, S. N. Fisher, A. M. Guenault, R. P. Haley, J. Kopu, H. Martin, G. R. Pickett, J. E. Roberts, and V. Tsepelin, Nat. Phys. **4**, 46 (2008).
[79] H. Takeuchi, K. Kasamatsu, M. Tsubota, and M. Nitta, Phys. Rev. Lett. **109**, 245301 (2012); J. Low Temp. Phys. **171**, 443 (2013); H. Takeuchi, K. Kasamatsu, M. Nitta, and M. Tsubota, *ibid.* **162**, 243 (2010).